CHEMISTRY
A European Journal

www.chemeurj.org

Reprint

A Journal of
ChemPubSoc Europe
ACES
Asian Chemical Editorial Society
WILEY-VCH

ChemPubSoc Europe

DOI: 10.1002/chem.201704923

CHEMISTRY
A European Journal
Communication

Epoxidation on Zeolites

Ethylene Epoxidation Catalyzed by Ag Nanoparticles on Ag-LSX Zeolites formed by Pressure- and Temperature-Induced Auto-Reduction

Donghoon Kim,[a] Yongmoon Lee,[a, b] Yonghwi Kim,[a] Kathleen Mingle,[c] Jochen Lauterbach,[c] Douglas A. Blom,[c] Thomas Vogt,[c, d] and Yongjae Lee*[a, b]

Abstract: Ag^+-Exchanged LSX (Ag-LSX: $Ag_{96}Al_{96}Si_{96}O_{384}{\cdot}n\,H_2O$), a large pore low silica analogue (Si/Al = 1.0) of faujasite, was prepared and post-synthetically modified using pressure and temperature in the presence of various pore-penetrating fluids. Using high-resolution synchrotron X-ray powder and single crystal diffraction we derive structural models of the as-prepared and post-synthetically modified Ag-LSX materials. In the as-prepared Ag-LSX model, we located 96 silver cations and 245 H_2O molecules distributed over seven and five distinctive sites, respectively. At 1.4(1) GPa pressure and 150 °C in ethanol the number of silver cations within the pores of Ag-LSX is reduced by ca. 47.4%, whereas the number of H_2O molecules is increased by ca. 40.8%. The formation of zero-valent silver nanoparticles deposited on Ag-LSX crystallites depends on the fluid present during pressurization. Ag-nanoparticle-Ag-zeolite hybrid materials are recovered after pressure release and shown to have different chemical reactivity when used as catalysts for ethylene epoxidation.

Zeolites are widely utilized in industry as ion-exchangers, sorbents, molecular sieves, and heterogeneous catalysts.[1] The members of the faujasite family display an unsurpassed performance in catalytic cracking of hydrocarbons and nitrogen/oxygen separation[2] and are classified into two sub-classes: X-types with a Si/Al ratio from 1 to 1.5 and Y-types with Si/Al ratios above 1.5. Amongst the X-type, low silica X (LSX) has a Si/Al ratio of 1 and the highest ion-exchange capacity.[3,4] In industrial applications, zeolites undergo thermal, compressional, and chemical changes, and understanding the systematic structural and compositional changes when exposed to temperature and pressure is crucial to modify and control properties as well as ensure prolonged performance as catalysts. A growing number of investigations using in situ temperature and pressure conditions have explored the cation-dependent dehydration and compression behavior of various X- and Y-type materials.[5]

Silver exchanged as a cation in zeolites leads to a number of materials with useful catalytic and adsorptive properties.[2b,6] Recently a metallic silver-containing hybrid zeolite material has been successfully synthesized by annealing the small-pore zeolite natrolite at moderate pressure and temperature conditions at 1.7(1) GPa and 250 °C.[8] This reaction under pressure and temperature can be rationalized using the auto-reduction model initially proposed by Jacobs (1979)[6e] in which the Ag^+ cations in the hydrated zeolite reacts with water and the framework oxygen to form gaseous O_2 and zero-valent Ag atoms. Using only heat as pointed out by Heo et al.,[6h] the auto-reduction leads to an amorphization of the zeolite framework which can be reversed by heating in O_2 or avoided by heating at elevated temperatures in flowing O_2. In Ag-Y zeolites, Tsutsumi et al. showed that nanocrystalline metallic silver particles are formed in Ag-Y zeolites after heat treatment above 600 °C in the presence of hydrocarbons.[9] Beyer et al.[6c] showed that the reduction mechanism of Ag in Y zeolites is dependent on temperature, and Gellens et al.[10] showed that cyclic reduction with hydrogen and oxidation with oxygen of Ag^+ ions in Y type zeolites depends on both redox conditions and temperature. In silver exchanged chabazite, the metallic silver particles are deposited on the surfaces of chabazite crystallites after heating at 150 °C.[11] We have extended our initial high-pressure investigation on natrolites to the large-pore zeolite LSX to establish pressure-induced auto-reduction in a large pore zeolite. Our first goal was to structurally characterize the recovered Ag_n-Ag-LSX hybrid materials containing mono- and zero-valent silver inside and outside of LSX crystallites, respectively. After distinct pressure and heat treatments of monovalent silver-exchanged low-silica X (Ag-LSX) and X (Ag-X) zeolites in the presence of different fluids used as pore-penetrating pressure-transmitting media, we derived structural models

[a] D. Kim, Dr. Y. Lee, Dr. Y. Kim, Prof. Dr. Y. Lee
Department of Earth System Sciences, Yonsei University
Seoul, 03722 (Korea)
E-mail: yongjaelee@yonsei.ac.kr

[b] Dr. Y. Lee, Prof. Dr. Y. Lee
Center for High Pressure Science and Technology Advanced Research
Shanghai 201203 (P. R. China)

[c] Dr. K. Mingle, Dr. J. Lauterbach, Dr. D. A. Blom, Prof. Dr. T. Vogt
NanoCenter and Department of Chemical Engineering
University of South Carolina
Columbia, SC 29208 (USA)

[d] Prof. Dr. T. Vogt
NanoCenter and Department of Chemistry and Biochemistry
University of South Carolina
Columbia, SC 29208 (USA)

Supporting information and ORCID(s) for the author(s) of this article can be found under:
https://doi.org/10.1002/chem.201704923.

of the as-prepared Ag-LSX and pressure-recovered hybrid Ag_n/Ag-LSX materials. Using scanning electron microscopy (SEM) with energy-dispersive X-ray spectroscopy (EDX), and high-angle annular dark-filed scanning transmission electron microscopy (HAADF-STEM), we confirmed that auto-reduction of monovalent silver cations in as-prepared Ag-LSX results in zero-valent silver particles deposited on Ag-LSX crsytallites. Silver and its oxides have been used as catalysts for ethylene epoxidation, and many computational studies probed the detailed reaction mechanisms of other oxidation processes.[7] Our second goal was to investigate the catalytic reactivity and selectivity of Ag_n/Ag-LSX hybrids using pressure- and temperature-induced reduction for ethylene epoxidation. Our goal was not to find optimized new catalysts for this reaction, by exploring established and possibly new promoters and modifiers, but to confirm that both conversion rate and selectivity of this reaction can be significantly impacted by rather simple post-synthetic modification, which increases the parameter space of such an optimization. The pressures we use are accessible in presses used to make KBr pellets for IR measurements.

In-situ high-pressure synchrotron X-ray powder diffraction (HPXRD) using a diamond anvil cell (DAC) was performed to explore the auto-reduction of Ag-LSX in the presence of different fluids (water, methanol, ethanol, acetone, benzene and toluene) (Figures 1 and S3a in the Supporting Information). The pressure measurement error is ± 0.1 GPa. Figure 1 shows the normalized intensity of the metallic silver (111) peak as a function of pressure in the presence of different fluids. The normalized intensity of the metallic silver (111) peak increases the most as pressure increases in the presence of methanol and ethanol. No phase transitions of the LSX material were observed in any fluid used to ensure hydrostatic pressure. The formation of nanocrystalline metallic Ag is promoted by pressure alone, in particular in the presence of methanol and ethanol. After pressure release and exposure to ambient conditions, metallic Ag ($Fm\bar{3}m$, $a = 4.08(1)$ Å) is still detected in the synchrotron X-ray pattern (Figure S3a) corroborating that metallic Ag nanoparticles formed without heating under pressure do not re-oxidize to monovalent silver at ambient conditions. Furthermore, the crystallinity of the zeolite framework is preserved in pressure-induced auto-reduction—this is in marked contrast to thermally-induced Ag nanoparticle formation.

To maximize Ag migration and retain the crystallinity of Ag-LSX, optimized temperature and pressure conditions (1.0(1) GPa and 150 °C) were used to synthesize Ag-LSX-P_{EtOH} using a large volume press (see the Supporting Information, Figure S3b). After a 1 hour dwelling time for Ag migration at 1.0(1) GPa and 150 °C, the samples were recovered and subjected to further characterization and experiments.

The PXRD profile of Ag-LSX-P_{EtOH} tracked the evolution of metallic Ag^0 nanoparticles from Ag-LSX by the growth of the (111) and (200) diffraction peaks of the cubic Ag^0 phase (Figure S3b in the Supporting Information). STEM images of Ag-LSX-P_{EtOH} also confirmed the formation of Ag^0 particles with sizes between 5 and 25 nm at the surface of Ag-LSX crystallites (see Figure 1).

Based on our Rietveld refinements the stoichiometry of Ag-LSX-P_{EtOH} is $Ag_{51(7)}Si_{96}Al_{96}O_{384}{\cdot}310(43)H_2O$, maintaining an Si/Al ordered framework with Si/Al = 1 crystallizing in a cubic unit cell ($Fd\bar{3}$) with $a = 24.982(2)$ (Table S2 in the Supporting Infor-

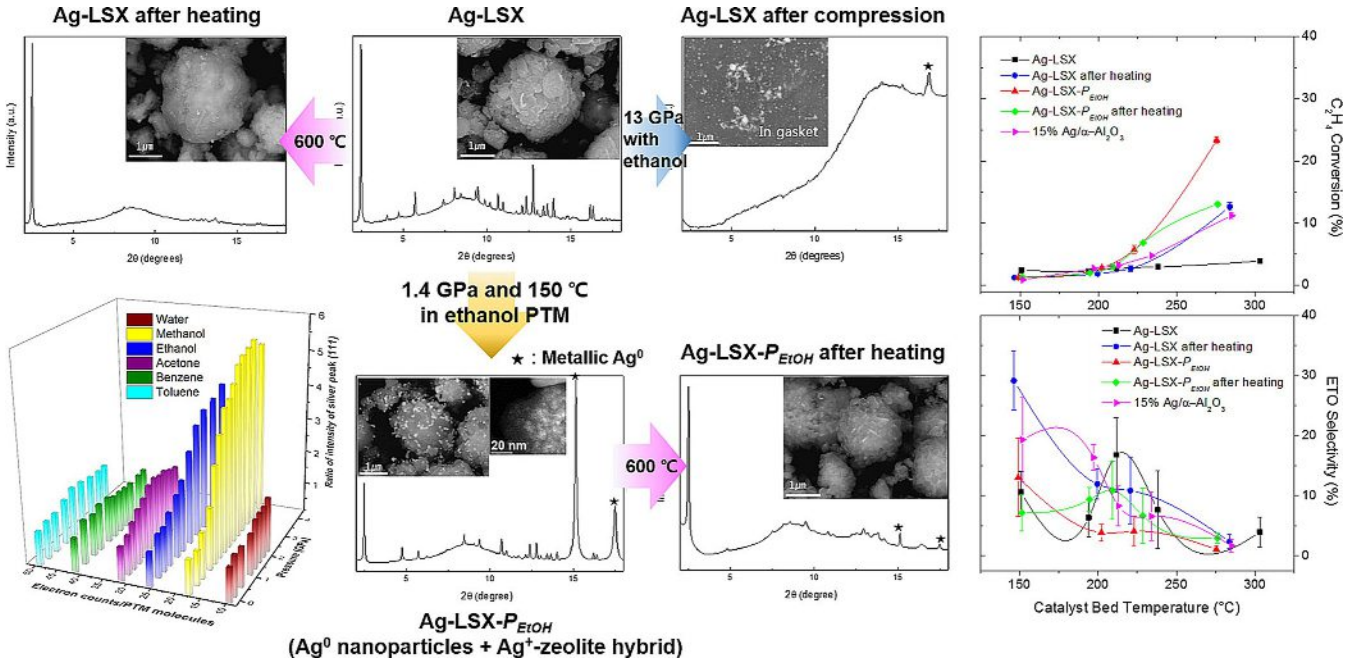

Figure 1. Morphological changes monitored by SEM and HAADF-STEM images and the corresponding synchrotron X-ray powder diffraction patterns of five samples with different post-synthetic pressure- and temperature-treatments. Left bottom shows the normalized intensity of the (111) reflection of metallic Ag as a function of pressure in the presence of different fluids (water, methanol, ethanol, acetone, benzene and toluene) measured by in situ high-pressure XRD using a diamond-anvil cell. Ethylene conversion and selectivity of different catalysts during epoxidation are shown on the right.

mation). The metallic Ag nanoparticles crystallizes in a cubic cell ($Fm\bar{3}m$) with $a = 4.0877(2)$. It is possible that the higher H_2O content in this model compared to that of Ag-LSX might be attributed to pressure-induced insertion of ethanol into the super-cages. However, due to the disordered distribution of the H_2O molecules we cannot distinguish pressure-inserted ethanol molecules from those of water using our current data. Furthermore, the charge balance of the Ag-LSX-P_{EtOH} sample $Ag_{51(7)}Si_{96}Al_{96}O_{384}{\cdot}310(43)H_2O$ calls for 45 framework protons, which due to the presence of water within the pores of the zeolite form according to: $2Ag_{96}Si_{96}Al_{96}O_{384} + 22.5H_2O \rightarrow$pressure$\rightarrow 11.25O_2 + 90Ag^0 + 2Ag_{51}H_{45}Si_{96}Al_{96}O_{384}$. Although this reaction is charge balanced, the error on the Ag content of Ag-LSX-P_{EtOH} indicates a range of possible redox reactions.

Ag^+ cations and H_2O molecules are found in six and seven distinctive crystallographic sites, respectively (Figures S6c,d in the Supporting Information). Compared to the Ag-LSX model, Ag-LSX-P_{EtOH} shows lower Ag occupancies at nearly all sites (Figure S6e). The number of silver ions at site I and I′ decreased from 15.0(1) to 10.4(3) and from 14.6(2) to 7.7(6), respectively (Tables S1 and S2 in the Supporting Information). The total number of silver ions at site II and II* also declined from 30(2) to 10(2). In the super-cage, the total number of silver ions at sites III′ decreased from 35(3) to 23(4), and the number of Ag sites also decreased from three to two.

For comparison, a single crystal of Ag^+-exchanged zeolite X ($Ag_{88}Al_{88}Si_{104}O_{384}{\cdot}n\,H_2O$) was prepared and characterized using X-ray diffraction. All diffraction peaks are indexed in the cubic space group $Fd\bar{3}m$, indicating a Si/Al disordered framework. During the structural analysis, about 91 silver ions were found in the unit cell of zeolite X (Table S5 in the Supporting Information). These Ag^+ ions were placed at five extra-framework sites with partial occupancies as follows: site I (91%), I′ (49%), II′ (4%), II* (83%), III′ (17%). However, after applying high pressure (0.7(1) GPa) and temperature (175 °C) to the crystal under ethanol PTM, the number of Ag in zeolite X was considerably reduced from 91(3) to 35(1), while maintaining the same space group (Table S5). Although there was little change in the occupancies of site I (91 to 90%) and II′ (4 to 9%), there were significant reductions of the occupancies in the other sites: site I′ (49 to 29%), II* (83 to 26%). After applying high pressure and temperature to a crystal of zeolite X strong diffraction peaks of Ag^0 were detected (Figure S5), which is in accordance with the results from the powder diffraction experiments on Ag-LSX (Figures 1 and S3 in the Supporting Information).

The PXRD pattern reveals that when heating the Ag-LSX-P_{EtOH} sample above 175 °C the amount of metallic silver gradually decreases (Figure 2a). This indicated that the Ag particles formed by pressure re-oxidize at higher temperatures. Some work has been done to reduce Ag^+ ions in X zeolites in hydrogen flow and re-oxidize Ag atoms in an oxygen flow, but the previously formed silver particles on the surface of X zeolites remained unchanged with oxygen flow at 473 K.[13] Based on in situ synchrotron X-ray diffraction data, the changes of the unit cell volume of Ag-LSX-P_{EtOH} as a function of temperature reveals three distinct regions (Figure S8a in the Supporting Information): the unit cell volume initially contracts from ambient to 125 °C, followed by an abrupt expansion between 125

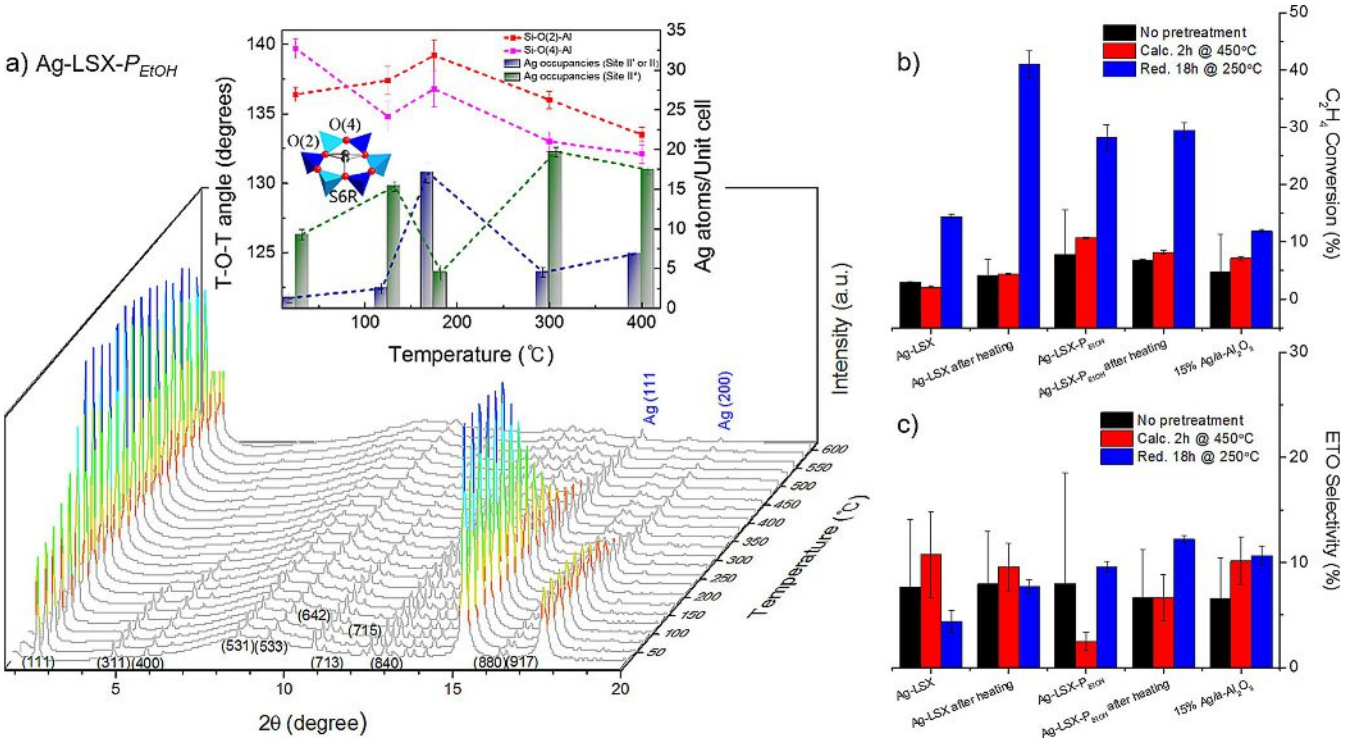

Figure 2. (a) Synchrotron X-ray powder diffraction patterns measured as a function of temperature for Ag-LSX-P_{EtOH}. The wavelength used was 0.6215(1) Å. Changes of the T-O-T bond angles and the number of Ag ions present in sites II, II′ and II* as a function of temperature. Further changes of (b) ethylene conversion and (c) selectivity rates when catalysts are treated in situ before the reactions.

and 175 °C, and a successive contraction until 600 °C. The overall unit cell volume contraction seems to be related to the gradual loss of H_2O (or pressure-inserted ethanol) as corroborated by the TGA (Figure S8b). An increased number of Ag ions at site II led to larger T-O(2)-T and T-O(4)-T angles, which are associated with the S6R (Tables S2, S4 in the Supporting Information and Figure 2a). This caused the anomalous expansion of the unit-cell volume between 125 and 175 °C. Above 175 °C, the gradual reduction of the unit cell volume is attributed to the reduced Ag occupancy in the site II and the steady removal of H_2O molecules as evidenced in the Ag-LSX-P_{EtOH}-300 and Ag-LSX-P_{EtOH}- 400 models (Table S2 and Figures 2 and S8).

To confirm the reversible redox reaction of metallic Ag and Ag-LSX, pressure- and temperature-treatments performed on the Ag-LSX-P_{EtOH}-*T* hybrid material after cooling from 600 °C to room temperature of Ag-LSX-P_{EtOH} in a DAC at 0.8(1) GPa and 150 °C, indicated that the metallic Ag particles are formed again (Figure S9 in the Supporting Information). Ag-LSX-P_{EtOH}-*TPT* (Ag-LSX-P_{EtOH}-*T* after pressure- and heat-treatment) was then heated inside a furnace (WiseTherm FH) at 300 °C and 500 °C for 1 hour. Ag-LSX-P_{EtOH}-*TPTT* (Ag-LSX-P_{EtOH}-*TPT* with heat-treatment) showed the reduction of the intensities of the diffraction peaks of metallic Ag particles. (Figure S9).

Figure 1 shows the morphological changes as seen in SEM and HAADF-STEM images and the corresponding X-ray diffraction pattern of different Ag-LSX materials using different post-synthetic pressure- and heat-treatments. The XRD pattern and SEM image shows no indications for metallic silver in the as-prepared Ag-LSX. A heat treatment up to 600 °C results in a collapsed and largely amorphous Ag-LSX phase and no formation of metallic silver nanoparticles. Ag-LSX-P_{EtOH} hybrid materials made by pressure- and heat-treatments at 1.4(1) GPa and 150 °C, respectively, contain silver nanoparticles observed in both SEM and HAADF-STEM images. The HAADF-STEM images and X-ray diffraction experiments reveal that a fraction of Ag^+ remains in the pores of Ag-LSX. Additional heating of the Ag-LSX-P_{EtOH} sample up to 600 °C reduces the amount silver nanoparticles on the Ag-LSC crystallites as corroborated by both XRD pattern and SEM images. Pressurizing Ag-LSX up to 13.0(1) GPa in the presence of ethanol results in a highly disordered zeolite material and Ag nanoparticles. Higher pressures thus trigger a pressure-induced amorphization. Amorphization is also observed at temperatures above 300 °C.

The catalytic activity of the hybrid materials depends on (1) the post-synthetic conditions used, such as heat treatment at 600 °C, and pressure treatment in the presence of ethanol as well as (2) the specific reaction conditions studied, such as reaction temperature and pretreatment conditions in the reactor. For all catalysts, C_2H_4 conversion increased with increasing temperature and remained under 5% at temperatures below 220 °C, as shown in Figure 1. Spline line fitting was used between experimental points on Figure 1 to guide the eye. Ag-LSX-P_{EtOH} exhibited the highest C_2H_4 conversion, with 23.3 ± 0.6% conversion at 275 °C, whereas Ag-LSX showed the lowest conversion with just 3.9 ± 0.2% at 303 °C. Conversely, Ag-LSX displayed the highest conversion among the four catalysts when the furnace set points were decreased to 150 °C. Ag-LSX-600 °C was the most selective catalyst studied, achieving 29.2 ± 4.9% ETO selectivity at 146 °C at a 1.2 ± 0.1% conversion rate, as shown in Figure 1. With the exception of the reaction data collected at 200 °C, Ag-LSX-600 °C consistently showed higher ETO selectivity than the standard 15% Ag/α-Al_2O_3 catalyst. Although Ag-LSX and Ag-LSX-600 °C were found to exceed the selectivity of the 15% Ag/α-Al_2O_3 catalyst under certain conditions, Ag-LSX-P_{EtOH} and Ag-LSX-P_{EtOH}-600 °C were on average less selective than all other catalysts studied, with Ag-LSX-P_{EtOH}-600 °C achieving a maximum ETO selectivity of just 10.9 ± 4.8% and a 3.0 ± 0.5% C_2H_4 conversion rate at a bed temperature of 209 °C. However, catalytic selectivity also varies with the conversion rate, and a direct comparison of selectivity is only meaningful at similar conversion rates. Furthermore, the industrial standard in ethylene oxide selectivity is close to 90%. As mentioned above, our catalyst does not contain alkali, rhenium, and no chlorine compounds were added to the feed as in industrial processes.

Catalytic performance at 250 °C was found to depend on whether the catalysts were exposed to an oxidative or reductive environment prior to testing, as shown in Figure 2. Figure 2b shows that the conversion increased significantly for all catalysts after an 18 hour reductive treatment at 250 °C with the lowest conversions were obtained when no pretreatment was used. Contrary to the results for the untreated and pre-calcined catalysts, in which Ag-LSX-P_{EtOH} achieved the highest conversion at 250 °C, Ag-LSX-600 °C converted the most C_2H_4 after the reductive pretreatment, with 41.0 ± 2.3%. Ag-LSX showed 10.8 ± 4.1% selectivity after the oxidative pretreatment, but this value dropped to 4.4 ± 1.1% after the reductive pretreatment. Ag-LSX-600 °C followed a similar trend, reaching 9.6 ± 2.2% conversion after calcination and decreasing to 7.7 ± 0.6% after reduction. All other catalysts reached their maximum selectivity after a reductive pretreatment. The highest selectivity achieved throughout all pretreatment experiments at 250 °C was 12.2 ± 0.4%, which was achieved by Ag-LSX-P_{EtOH}-600 °C after reductive treatment.

We have shown that post-synthetic modifications of Ag-LSX using temperature and pressure in the presence of various fluids results in the formation of a wide variety of Ag_n/Ag-LSX hybrid materials. Our structural work establishes the different Ag-LSX structures present in, that is, Ag-LSX-P_{EtOH} and confirms that Ag^+ ions in the zeolite migrate during the post-synthetic treatment to form Ag^0 nanoparticles on the surfaces of the zeolite crystallites. The degree of crystallinity of the Ag-LSX material and the amount of Ag nanoparticles on their surfaces can be controlled. We also note that the type of fluid plays a role in the pressure treatment. This provides an alternative route for a non-thermal in situ formation of Ag nanoparticles on zeolite crystallite surfaces. Pressure-driven in situ synthesis of metallic nanoparticles on the surface of zeolite crystallites should be explored in other systems as it provides an alternative route to thermal and/or physical deposition and is highly reproducible.

The catalytic reactivity and selectivity of various Ag_n/Ag-LSX hybrids during ethylene epoxidation (ETO) clearly establishes the importance of pressure- and temperature-induced post-

synthetic modifications. As expected, the different morphologies depicted in Figure 1 impact the chemical reactivity. At temperatures above 225 °C, the pressure-driven post-synthetic modification results in the highest C_2H_4 conversion comparable to those of a non-optimized 15% Ag/α-Al_2O_3 catalyst. The subsequent loss of crystallinity found in hybrid materials which were heated up to 600 °C reduces the C_2H_4 conversion to the level of the 15% Ag/α-Al_2O_3 catalyst and other post-synthetically modified hybrids. The observed changes in C_2H_4 conversion and ETO selectivity make the case that taking an appropriately cation substituted zeolite and exploring post-synthetic modifications using both pressure and temperature is a promising strategy to create new heterogeneous metallic nanoparticles on zeolites as support. This should further intensify the use of post-synthetic modifications in high-throughput studies of heterogeneous catalysts. Additional in situ treatment of the catalysts reveals that a prolonged reduction over 18 hours at 250 °C results in significant changes of the conversion rate. In particular, the heat-treated Ag-LSX-600 °C increases its C_2H_4 conversion rate, as do the pressure-treated Ag-LSX-P_{EtOH} and pressure- and heat-treated Ag-LSX-P_{EtOH}-600 °C while maintaining their selectivity.

We show that under hydrostatic pressure in the presence of pore-penetrating methanol and ethanol auto-reduction of Ag-LSX to Ag-nanoparticle-Ag^+-zeolite hybrid materials occurs at moderate temperatures, while maintaining the framework crystallinity and morphology. Intriguing future possibilities are the formation of bi-metallic nanoparticles by appropriate cation substitution in the zeolites and the exploration of reactions requiring metals in zero and higher oxidation states.

Acknowledgements

This work was supported by the Global Research Laboratory (NRF-2009-00408) and National Research Laboratory (NRF-2015R1A2A1A01007227) programs of the Korean Ministry of Science, ICT and Planning (MSIP). We also thank the supports by NRF-2016K1A4A3914691 and NRF-2016K1A3A7A09005244 grants. Experiments using X-ray synchrotron radiation were supported by the Pohang Accelerator Laboratory (PAL). The JEOL 2100F is supported by the Office of Research at the University of South Carolina.

Conflict of interest

The authors declare no conflict of interest.

Keywords: ag-lsx · auto-reduction · catalyst · ethylene epoxidation · post-synthesis · pressure/ temperature

[1] a) F. Bouchet, H. Fujisawa, M. Kato, T. Yamaguchi, *Stud. Surf. Sci. Catal.* **1994**, *84*, 2029 – 2036; b) D. W. Breck, *New York: John Wiley and Sons* **1974**; c) R. M. Barrer, *London: Academic Press* **1978**.

[2] a) A. Maes, A. Cremers, *J. Chem. Soc. Faraday Trans. 1* **1975**, *71*, 265 – 277; b) H. S. Sherry, *J. Phys. Chem-US* **1966**, *70*, 1158 – 1168; c) C. J. Plank, E. J. Rosinski, W. P. Hawthorne, *Ind. Eng. Chem. Prod. Rd.* **1964**, *3*, 165 – 169; d) S. Yoshida, S. Hirano, A. Harada, M. Nakano, *Microporous Mesoporous Mater.* **2001**, *46*, 203 – 209; e) M. L. Zanota, N. Heymans, F. Gilles, B. L. Su, M. Frère, G. De Weireld, *J. Chem. Eng. Data* **2010**, *55*, 448 – 458; f) D. Shen, M. Bülow, S. R. Jale, F. R. Fitch, A. F. Ojo, *Microporous Mesoporous Mater.* **2001**, *48*, 211 – 217.

[3] G. H. Kühl, *Zeolites* **1987**, *7*, 451 – 457.

[4] Y. Lee, S. W. Carr, J. B. Parise, *Chem. Mater.* **1998**, *10*, 2561 – 2570.

[5] a) Y. Lee, H. L. Hyun, R. L. Dong, J. S. Tae, J. Y. Choi, C. C. Kao, *J. Am. Chem. Soc.* **2007**, *129*, 4888 – 4889; b) R. Khaleghian-Moghadam, F. Seyedeyn-Azad, *Microporous Mesoporous Mater.* **2009**, *120*, 285 – 293; c) U. D. Joshi, P. N. Joshi, S. S. Tamhankar, V. P. Joshi, B. B. Idage, V. V. Joshi, V. P. Shiralkar, *Thermochim. Acta* **2002**, *387*, 121 – 130; d) B. Beagley, J. Dwyer, F. Fitch, M. A. Zanjanchi, *J. Inclusion Phenom.* **1985**, *3*, 143 – 149; e) G. N. D. Al-Ajdah, A. A. Al-Rished, B. Beagley, J. Dwyer, F. R. Fitch, T. K. Ibrahim, *J. Inclusion Phenom.* **1985**, *3*, 135 – 142; f) M. Colligan, P. M. Forster, A. K. Cheetham, Y. Lee, T. Vogt, J. A. Hriljac, *J. Am. Chem. Soc.* **2004**, *126*, 12015 – 12022.

[6] a) L. Martins, R. T. Boldo, D. Cardoso, *Microporous Mesoporous Mater.* **2007**, *98*, 166 – 173; b) L. R. Gellens, W. J. Mortier, J. B. Uytterhoeven, *Zeolites* **1981**, *1*, 11 – 18; c) H. Beyer, P. A. Jacobs, J. B. Uytterhoeven, *J. Chem. Soc. Faraday Trans.* **1976**, *72*, 674 – 685; d) P. A. Jacobs, J. B. Uytterhoeven, H. K. Beyer, *J. Chem. Soc. Faraday Trans.* **1977**, *73*, 1755 – 1762; e) P. A. Jacobs, J. B. Uytterhoeven, H. K. Beyer, *J. Chem. Soc. Faraday Trans.* **1979**, *75*, 56 – 64; f) L. R. Gellens, W. J. Mortier, R. A. Schoonheydt, J. B. Uytterhoeven, *J. Phys. Chem-US* **1981**, *85*, 2783 – 2788; g) M. D. Baker, G. A. Ozin, J. Godber, *J. Phys. Chem.* **1984**, *88*, 4902 – 4904; h) N. H. Heo, Y. Kim, J. J. Kim, K. Seff, *J. Phys. Chem. C* **2016**, *120*, 5277 – 5287.

[7] a) A. Kokalj, P. Gava, S. de Gironcoli, S. Baroni, *J. Catal.* **2008**, *254*, 304 – 309; b) K. C. Waugh, M. Hague, *Catal. Today* **2010**, *157*, 44 – 48; c) M. O. Ozbek, I. Onal, R. A. Van Santen, *J. Catal.* **2011**, *284*, 230 – 235; d) M. C. N. Amorim de Carvalho, F. B. Passos, M. Schmal, *J. Catal.* **2007**, *248*, 124 – 129.

[8] D. Seoung, Y. Lee, H. Cynn, C. Park, K. Y. Choi, D. A. Blom, W. J. Evans, C. C. Kao, T. Vogt, Y. Lee, *Nat. Chem.* **2014**, *6*, 835 – 839.

[9] K. Tsutsumi, H. B. Takahashi, *Bull. Chem. Soc. Jpn.* **1972**, *45*, 2332 – 2337.

[10] L. R. Gellens, W. J. Mortier, J. B. Uytterhoeven, *Zeolites* **1981**, *1*, 85 – 90.

[11] S. M. Kuznicki, D. J. A. Kelly, J. Bian, C. C. H. Lin, Y. Liu, J. Chen, D. Mitlin, Z. Xu, *Microporous Mesoporous Mater.* **2007**, *103*, 309 – 315.

[12] a) D. A. Robb, P. Harriott, *J. Catal.* **1974**, *35*, 176 – 183; b) P. A. Kilty, W. H. Sachtler, *Catal. Rev.* **1974**, *10*, 1 – 16.

[13] M. Iwamoto, T. Hashimoto, T. Hamano, S. Kahawa, *Bull. Chem. Soc. Jpn.* **1981**, *54*, 1332 – 1337.

Manuscript received: October 17, 2017
Accepted manuscript online: December 14, 2017
Version of record online: January 12, 2018